Joint Communication and Sensing Design in Coal Mine Safety Monitoring: 3-D Phase Beamforming for RIS-Assisted Wireless Networks

Tianhao Guo, *Member, IEEE*, Xianzhong Li, Muyu Mei, Zhaohui Yang, *Member, IEEE*, Jia Shi, *Member, IEEE*, Kai-Kit Wong, *Fellow, IEEE*, and Zhaoyang Zhang, *Senior Member, IEEE*

***Abstract*—This article investigates the resource allocation of a reconfigurable intelligent surface (RIS)-aided joint communication and sensing (JCAS) system in a coal mine scenario. In the JCAS system, an RIS is implemented at the corner of the zigzag tunnels to improve the complicated wireless environment, where ground obstacles frequently block direct links. In addition, a wireless backhaul base station with a limited energy budget is deployed in the depth of the mine to sense the target area and provide Internet of Things (IoT) services and communication services for users. Furthermore, a data center is placed on the ground to analyze the obtained data and route the communication data. Under this deployment, a joint optimization problem of RIS phase-shift matrix, RIS element switches, and area sensing time is proposed. We aim to maximize the successful sensed bits under total completion time, and maximum transmit power constraints. In order to solve this problem, an iterative algorithm is proposed. The successive convex approximation (SCA)-based algorithm is used for the RIS phase-shift matrix optimization subproblem. For the sensing time optimization subproblem, the quadratic approximation method is proposed to optimize the number of area perceptions. The coordinate descent method is utilized to optimize the RIS element switches. Simulation results show that the energy efficiency is improved by up to 38%, and 7% increases the specific data size compared with the benchmark solutions.**

***Index Terms*—Energy efficiency, joint communication and sensing (JCAS), reconfigurable intelligent surface (RIS), safety monitoring schedule.**

I. Introduction

With the rapid development of wireless networks, spectrum resources are becoming congested. High-frequency bands are exploited and investigated to meet the increasing demand of wireless networks, including radar bands. Due to the similar properties of the occupied frequency bands, radar and communication systems have many overlaps in system models, channel characteristics, and signal processing design. Integrating radar and communication can improve efficiency (integration gain [1]) of resources, e.g., spectrum, energy, and device cost (also reducing weight for drones [2]).

Radar signals can be modulated, while wireless communication is also built based on identification and authentication. The integration of sensing and communication is not only an improvement or extension of existing communication technologies but also a paradigm revolution. As the neural system of animals, sensing the environment and transmitting information are two essential functions. By combining communication and sensing, human beings can build the neural system of the physical world and the intelligent world.

Millimeter-wave (mmWave) bands have been officially adopted in fifth-generation (5G) cellular systems. Adopting high-frequency bands brings wide bandwidth and increases detection resolution [3] by more than two orders of magnitude (to 0.1 mm or less) [4]. Moreover, the "pencil-like" [5] mmWave beams suffer from only a few multipath target echoes, which means far less clutter interference. In other words, the future networks can clearly "see" the world. In the 6G era, the positioning accuracy is expected to be 10 cm (indoor) and 1 m (outdoor) [6]. With the large-scale deployment of cellular networks, there are increasing emerging sensing-enabled applications for future networks. Solid applications include high-resolution indoor positioning [7], navigation, and even high-resolution computational imaging, extending perception range beyond the line of sight in vehicular networks.

Manuscript received 30 July 2022; revised 29 December 2022; accepted 23 January 2023. Date of publication 9 February 2023; date of current version 23 June 2023. This work was supported in part by the Zhejiang Key Research and Development Program under Grant 2023C01021; in part by the National Key Research and Development Program of China under Grant 2020YFB1807101 and Grant 2018YFB1801104; and in part by the National Natural Science Foundation of China under Grant U20A20158, Grant 61725104, and Grant 61825104. *(Corresponding author: Zhaohui Yang.)*

Tianhao Guo is with the Department of Physical and Electronic Engineering, Shanxi University, Taiyuan 030006, China, and also with the State Key Laboratory of Integrated Services Networks, Xidian University, Xi'an 710071, China (e-mail: tianhao_guo@sxu.edu.cn).

Xianzhong Li is with the Department of Physical and Electronic Engineering, Shanxi University, Taiyuan 030006, China (e-mail: 2843475772@qq.com).

Muyu Mei is with the State Key Laboratory of Integrated Services Networks, School of the Telecommunication Engineering, and the Guangzhou Institute, Xidian University, Xi'an 710071, China (e-mail: mei_muyu@163.com).

Zhaohui Yang is with the Department of Information Science and Electronic Engineering Zhejiang Key Laboratory of Information Processing Communication and Networking, Zhejiang University, Hangzhou 310027, China, and also with the Research Institute of Intelligent Networks, Zhejiang Laboratory, Hangzhou 311121, Zhejiang, China (e-mail: yang_zhaohui@zju.edu.cn).

Jia Shi is with the State Key Laboratory of Integrated Services Networks, Xidian University, Xi'an 710071 China (e-mail: jiashi@xidian.edu.cn).

Kai-Kit Wong is with the Department of Electronic and Electrical Engineering, University College London, WC1E 6BT London, U.K. (e-mail: kai-kit.wong@ucl.ac.uk).

Zhaoyang Zhang is with the College of Information Science and Electronic Engineering, Zhejiang University, Hangzhou 310027, China (e-mail: zhzy@zju.edu.cn).

Digital Object Identifier 10.1109/JIOT.2023.3242340

Among those applications, coal mining is a vertical industrial application where 5G/6G networks are promising to land. The standard requirements of industrial networks are low latency [8], [9], [10], indoor positioning, large-scale connections, and low power consumption [11]. In addition to these typical requirements, the unique requirement of coal mining is safety monitoring. This is due to the three unique properties of coal mining: 1) water seepage; 2) goaves; and 3) toxic and explosive gases.

1) Electromagnetic waves in the mmWave bands and higher bands experience a severe loss, especially in an environment with high-humidity air. However, the disadvantages of communication can be the advantages of perception. Once it is found that the radar echo in a specific area of the tunnel has an unknown loss, an unmanned vehicle can be sent to check.
2) The goaf is a "cavity" created by artificial excavation or natural geological movement, which can cause severe loss of properties and human lives. The spatial location of the goaves is concealed and randomly distributed. Besides, the roof collapse of the goaf is uneasy to be predicted. The joint communication and sensing (JCAS) system is able to predict the danger and effectively detect it. Moreover, once people and equipment fall into the goaf, the structure inside the goaf can be "seen" through electromagnetic inverse scattering imaging technology [12], so rescue can be carried out in time.

This article considers a small battery-powered wireless backhaul JCAS base station that can transmit the sensory data to the data center (DC) for further processing. From the system design point of view, time-division sensing and communication integrated system [2] is more suitable for power-constraint scenarios. In order to ensure the freshness of the sensory data, the interval (sensing phase) between two successive communication phases should be short. However, there should also be enough time for sensing to ensure data accuracy and to send the sensory and communication data. Hence, the tradeoff between the sensing and transmission phase with the constraints of sensing and communication demands was optimized in this article.

Reconfigurable intelligent surface (RIS), as a candidate technology of 6G, is also promising to be applied in coal mines [13], [14], [15], [16], [17], [18]. The reasons are as follows.

1) Interference can be controlled for RIS communications.
2) It is easy to implement and manage RIS in tunnels of coal mines.
3) RIS is an economical and green way [19] to transmit data through winding tunnels (multihop RIS [20]).
4) Since each element can independently control the incident signal, by continuously adjusting the reflection characteristics, the receiver can obtain different echo signals, thereby obtaining more environmental information.
5) The high spreading loss and molecular absorption often limit [21] the signal transmission distance and coverage range of mmWave and THz bands, while massive multiple input–multiple output (MIMO) [21] and multihop RIS [20] can help combat the distance issue.
6) If accident happens, some hops of the RIS may encode the information of the place and the reason of the accident in the frontier of the mine.
7) If multiple antennas are too close, it will reduce the resolution of perception and cause the loss of matrix rank. RIS can be utilized in a distributed multiantenna system, which can be considered to increase the aperture of the radar.

Although the utilization of RIS in coal mines is beneficial, there are still some open issues regarding integration. Among these issues, we focus on two vital questions in this work.

1) *Question 1:* Is time-division sensing and communication feasible for security checks in coal mines?
2) *Question 2:* Is it feasible to use RIS to assist wireless communications in coal mines?

We are devoted to answering these two questions in this work, and the results are summarized in the following contributions of this work.

1) The RIS-assisted JCAS system in the coal mine scenario is modeled, and the allocation strategy of sensing time and communication time is optimized. The simulation results show that the JCAS system can perceive as much sensory data as possible by reasonably allocating sensing and communication time in coal mines to ensure mine safety.
2) RIS is deployed in the coal mine tunnels, and the RIS phase-shift matrix is optimized to improve the communication rate. After the optimization of 3D-RIS, the energy efficiency is further improved, which verifies the feasibility of RIS-assisted communications in the coal mine tunnels.

The remainder of this article is organized as follows. Section II presents the related works of JCAS and RIS. Section III introduces the system model of this article. Section IV provides the problem formulation. Simulation results are provided in Section V, and Section VI concludes this article.

II. Related Works

A. Related Works on Safety Monitoring in Coal Mines

Safety monitoring of the tunnel environment needs a high sampling density of data, which needs to deploy many traditional sensors to different places and upload data on time. Usually, we tend to use wires to bridge sensing points to gather data at processing servers. However, wired networks are less scalable because sensors must be deployed as the tunnel advances. In contrast, wireless sensor networks (WSNs) are scalable for tunnel environments, and multihop routing is necessary for WSNs because direct wireless transmission is unfeasible in winding tunnels [22]. WSNs routing protocols and sensor nodes deployment have been studied in various cases [22], [23]. However, the cost of device deployment and maintenance for WSNs is still high, and WSNs are unable to integrate industrial network services directly into the coal mine.

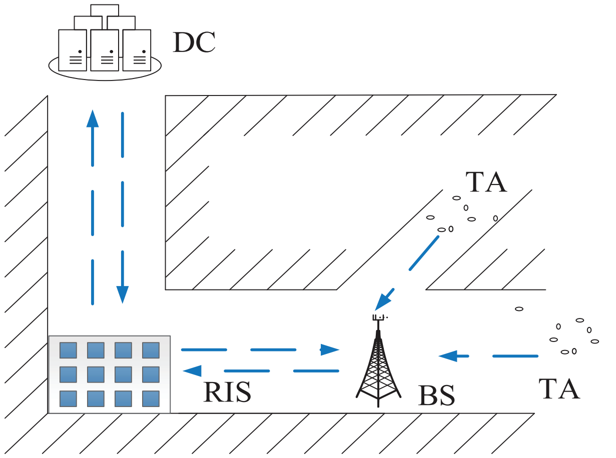

Fig. 1. System model of coal mine sensing and communication.

Wireless electromagnetic wave attenuation characteristics for underground coal mines are studied in various cases (rock roughness [24] and dust concentration), but this kind of research is only suitable for ultrahigh frequency (300 MHz–3 GHz). The performance of the MIMO system operating at 60 GHz (mmWave) is studied in the real-world underground gold mine [25] in Quebec, Canada. For a 2 × 2 MIMO system, the channel capacity can reach at least 4 bits/s/Hz.

Sensing is the foundation of mechanized and automated mining systems. 2-D or 3-D profiling visualization systems enabled by mmWave or laser have been implemented in underground and surface mines in Australia and South Africa decades ago [26], [27], [28]. By monitoring the 2-D and 3-D cloud images of mining vehicles [26], [27], tunnels, and dig areas, automation and safety can be guaranteed to some extent. Those systems above have no communication functions.

B. Related Works on Integrated Sensing and Communication

From the signal processing point of view, the radar can modulate communication information on the radar electromagnetic waves, such as pulse interval [29] and sidelobe of the MIMO radar beampattern [30]. On the other hand, the base station can also use its own reflected (echo) signals [31] to detect blockages, such as walls because blockage can "modulate" signals by reflections. By collecting multipath uplink signals from other devices with the aid of RIS, the pixel blocks (computational imaging) of the surroundings can be reconstructed [32], [33].

III. System Model

In this article, we consider a wireless JCAS system, wherein data is sensed from a set $\mathbb{K}$ of K different target areas (TAs), and the sensory data is transmitted to a DC with the help of a RIS to tackle the blockage of the cave, as shown in Fig. 1. The RIS has N reflecting elements and can be controlled through a diagonal matrix $\boldsymbol{\Theta} = \mathrm{diag}(e^{j\theta_1}, \ldots, e^{j\theta_N}) \in \mathbb{C}^{N\times N}$ with $\theta_l \in [0, 2\pi]$ and $j = 1, \ldots, N$.

The notations and meanings appearing in this article are summarized in Table I. In order to sense different areas, the JCAS transmitter should be able to change the direction, and

TABLE I
List of Notations for Problem Formulation

Notations	Meanings
T	Data update time.
t	Communication time.
D_k	Total perceived data of the k_{th} area.
b_k	Perceptual number sequence.
N	Number of RIS units.
n	Background noises.
K	The number of target areas.
t_0	The basic sensing slot.
q_k	Probability of success for sensing k_{th} area.
ϵ	Perceived probability coefficient.
d_k	Distance from the BS to the target area.
M	Number of base station antennas.
b_{opt}	Optimal perceptual times sequence

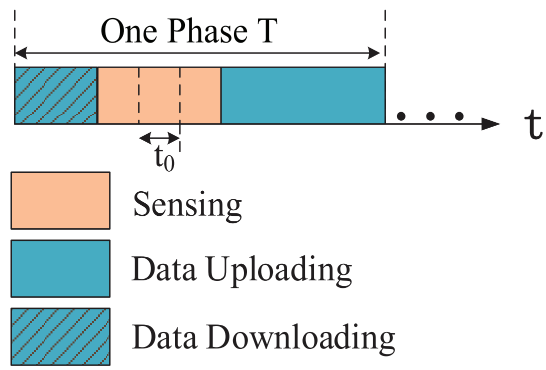

Fig. 2. Time allocation of one phase T.

the beamforming vector is denoted by $\boldsymbol{\omega}$. The received signal at the DC is

$$y = \left(\boldsymbol{g}^H + \boldsymbol{h}^H \boldsymbol{\Theta} \boldsymbol{G}\right)\boldsymbol{\omega} + n \tag{1}$$

where $\boldsymbol{g} \in \mathbb{C}^M$, $\boldsymbol{G} \in \mathbb{C}^{N\times M}$, and $\boldsymbol{h} \in \mathbb{C}^N$ denote the channel responses from the transmitter to the DC, from the transmitter to the RIS, and from the RIS to the DC, respectively. In (1), $n \sim \mathcal{CN}(0, \sigma^2)$ is the additive white Gaussian noise.

The JCAS system needs to sense K TAs and transmit the data repeatedly to ensure the freshness [2] of the sensory data. As shown in Fig. 2, a period T consists of a downloading phase (control and downloading data from DC to BS), a sensing phase, and an uploading phase (sensory data and communication data from BS to DC). Note that K TAs have different conditions and security requirements, so the sensing priorities (sensing periods) may vary. The primary sensing slot of a TA is t_0, and the sensing duration t_k of kth TA within a sensing phase is $b_k t_0$. The task completion probability of a TA in a sensing slot is [2]

$$q_k = e^{-\epsilon d_k} \tag{2}$$

where ϵ_k is the perceived probability coefficient and d_k is the distance from the BS to the TA. The task completion probability of a TA in a sensing duration is

$$P_k = 1 - (1 - q_k)^{b_k}. \tag{3}$$

The transmission (uploading and downloading) duration within a sensing phase is given by

$$t = \frac{\sum_{k=1}^{K} P_k D_k + D_f}{B\log_2\left(1 + \frac{\|g^H + h^H \Theta G)\omega\|^2}{\sigma^2}\right)} \tag{4}$$

where D_k is the data size of the kth TA and B is the bandwidth. The size of uploading and downloading data is fixed to D_f. In order to formalize the problem, the mathematical expectation of the total data is used to approximate the sensed total data, expressed as $P_k \cdot D_k = P_k \cdot D_k + (1 - P_k) \cdot 0$.

Our objective is to jointly optimize the reflection coefficient matrix $\mathbf{\Theta}$ and sensing times b_k of the kth TA to maximize the overall size of the sensory data under the data freshness requirements and the total power-constraint $\boldsymbol{P}_{\max}$. The problem can be formulated as follows:

$$\max_{\boldsymbol{b},\boldsymbol{\theta}} \sum_{k=1}^{K} P_k D_k \tag{5}$$

$$\text{s.t.} \quad \left(\sum_{k=1}^{K} b_k\right) t_0 + t \leq T \tag{5a}$$

$$P_k \geq Q_k, \quad k = 1, 2, 3 \ldots, K \tag{5b}$$

$$\boldsymbol{\theta} \in [0, 2\pi] \tag{5c}$$

$$b_k \in N^+. \tag{5d}$$

The freshness constraint is guaranteed by (5a), where sensing duration $\sum_{k=1}^{K} b_k t_0$ plus transmitting duration are not allowed to exceed the period T to ensure the freshness of the sensory data. The task completion probability needs to satisfy the security requirements [Q_k in (5b)]. That is, (5b) guarantees the basic security requirement (Q_k) of each TA. On this basis, we try to improve the accuracy of sensing, so as to improve the security. For the sake of the sensing quality, we set a minimum successful sensing probability threshold Q_k for the BS. The power constraint is provided in (5c).

Batteries provide power for the BS and the RIS in the coal mine. When there are abundant RIS elements, the energy consumed by the RIS to regulate the phase is unignorable, even if the single RIS energy consumption is low. In order to further improve the energy efficiency, we add switch vectors to RIS elements and strive to find the optimal switch combination to further improve the energy efficiency.

The amplitude of RIS elements is controlled by the $\boldsymbol{x}$ vector, $\boldsymbol{x} = [x_1, \ldots, x_N]^T$, so as to realize the 3-D control of RIS elements. The 3D-RIS optimization problem can be expressed by the following problem:

$$\max_{\boldsymbol{x}} \; y = \boldsymbol{\omega}\left(\boldsymbol{g^H} + \boldsymbol{h^H X \Theta G}\right) + n \tag{6}$$

$$\text{s.t.} \quad x_1, \ldots, x_N \in \{0, 1\} \tag{6a}$$

where $\boldsymbol{X} = \text{diag}(\boldsymbol{x}^T) \in \mathbb{R}^N$. Since the problem has been formulated under the system model we presented in this section, we proceed to Section IV.

Algorithm 1 SCA Method

Initialize $\boldsymbol{v}^{(0)}$, set iternumber $n = 1$.
repeat
set $\boldsymbol{v}^{(j)} = e^{-j\angle(\boldsymbol{U}(\boldsymbol{g}+\boldsymbol{U}^H\boldsymbol{\theta}^{(j-1)}))}$, and, $j = j + 1$.
until the objective value converges, $\boldsymbol{\theta} = (\boldsymbol{v}^{(j)})^*$.

IV. Problem Formulation

Problem (5) is nonconvex, and it is generally hard to obtain the global optimal solution, so (5) is divided into two subproblems. First, we optimize the RIS phase to maximize the channel gain. Second, we optimize the perceptual time allocation problem.

A. Phase Optimization

In this section, we are devoted to solving the first step. When $\boldsymbol{X}$ is an identity matrix, the phase-shift matrix optimization problem can be expressed as

$$\max_{\boldsymbol{\theta}} \; y = \boldsymbol{\omega}\left(\boldsymbol{g^H} + \boldsymbol{h^H \Theta G}\right) + n \tag{7}$$

$$\text{s.t.} \quad \theta_j \in [0, 2\pi], j = 1, \ldots, N \tag{7a}$$

where $\boldsymbol{\theta} = [e^{j\theta_1}, \ldots, e^{j\theta_N}]^T$. From the objective function (7) and the constraint in (7a), we observe that the optimal $\boldsymbol{\theta}$ is the one that maximizes the channel gain. Before optimizing $\boldsymbol{\theta}$, we notice that $h^H \mathbf{\Theta} = \boldsymbol{\theta}^T \text{diag}(\mathbf{h}^H)$. According to problem (6), the optimal $\boldsymbol{\theta}$ can be calculated by solving the following problem:

$$\max_{\boldsymbol{\theta}} \; y = |\boldsymbol{g} + \boldsymbol{U^H v}|^2 \tag{8}$$

$$\text{s.t.} \quad |\boldsymbol{v}_j| = 1, j = 1, \ldots, N \tag{8a}$$

where $\mathbf{U} = \text{diag}(\mathbf{h}^H)\mathbf{G}$ and $\boldsymbol{v} = \boldsymbol{\theta}^*$. This article uses the successive convex approximation (SCA) method to optimize the problem (8), and the alternating optimization algorithm is the comparison algorithm.

Under the SCA approach, problem (8) can be approximated as

$$\max_{\boldsymbol{\theta}} \; 2R\left(\left(\boldsymbol{g} + \boldsymbol{U}^H\boldsymbol{v}^{(j-1)}\right)^H \boldsymbol{U}^H\boldsymbol{v}^j\right) - |\boldsymbol{g} + \boldsymbol{U}^H\boldsymbol{v}^{(j-1)}|^2 \tag{9}$$

$$\text{s.t.} \quad |\boldsymbol{v}_j| = 1, j = 1, \ldots, N. \tag{9a}$$

Lemma 1: In problem (9), the optimal solution is

$$\boldsymbol{v}_{\text{opt}} = e^{-j\angle(\boldsymbol{U}(\boldsymbol{g}+\boldsymbol{U}^H\boldsymbol{v}^{(j-1)}))}. \tag{10}$$

Proof: $\angle(\boldsymbol{U}(\boldsymbol{g} + \boldsymbol{U}^H\boldsymbol{v}^{(j-1)}))$ denotes the phase of $(\boldsymbol{U}(\boldsymbol{g} + \boldsymbol{U}^H\boldsymbol{v}^{(j-1)}))$. When the phase of $(\boldsymbol{g} + \boldsymbol{U}^H\boldsymbol{\theta}^{(n-1)})\boldsymbol{U}^H$ and $\boldsymbol{v}$ us opposite, the value of the objective function can be optimized, and (10) is the optimal solution. The SCA algorithm for solving problem (8) is summarized in Algorithm 1.

For comparison, we alternatively optimize the phase of one element in RIS and fix the phase angle of other elements. This method decomposes the multidimensional optimization problem into multiple 1-D optimization problems to simplify the calculation. The detailed steps are shown in Algorithm 2. ■

Algorithm 2 Alternating Optimization Algorithm

Initialize $\theta_j = 0, j = 1 : N$.
repeat
  for $j = 1, \ldots, N$
    $\theta_j = argmax(y)$.
  endfor
until the obiective value converges.

B. Sensing Time Optimization

There are multiple TAs, and the size of sensory data in each TA varies for the coal mine scenario. Each TA's perceived probability needs to cater for the probability constraint due to different perceived priorities. The system's optimal sensing time allocation strategy needs to be obtained first.

As observed, problem (5) is a nonconvex problem, which needs to be further transformed into a convex problem to be solved. This article uses the Taylor quadratic approximation method to solve the relaxation problem corresponding to the original integer programming problem for the perceptual time allocation problem. Replacing (2) into objective function in problem (5), we can obtain the following expression:

$$y = \sum_{k=1}^{K} \left[1 - (1 - q_k)^{b_k}\right] \cdot D_k. \tag{11}$$

Then, we let $Q_k = 1 - q_k$ and the objective function can be rewritten as $y = \sum_{k=1}^{K} [1 - {Q_k}^{b_k}] \cdot D_k$. Furthermore, the objective function is expanded to $y = \sum_{k=1}^{K} D_k - \sum_{k=1}^{K} {Q_k}^{b_k} \cdot D_k$ and $\sum_{k=1}^{K} D_k$ is the fixed value. Let $y_1 = \sum_{k=1}^{K} {Q_k}^{b_k} \cdot D_k$, y_1 becomes the new objective function. According to the Taylor expansion $a^x = \sum_{n=0}^{N} (xlna)^n/n!$, the objective function can be approximated as $y_1 = \sum_{k=1}^{K} [1 + b_k lnQ_k + (b_k lnQ_k)^2/2] \cdot D_k$. Letting $y_2 = \sum_{k=1}^{K} [b_k lnQ_k + (b_k lnQ_k)^2/2] \cdot D_k$, the optimization problem (12) is obtained by expressing y_2 in a matrix form

$$\min_{\mathbf{b}} \; y_2 = \mathbf{a}^T \cdot \mathbf{b} + \mathbf{b}^T \cdot \mathbf{A} \cdot \mathbf{b} \tag{12}$$

$$\text{s.t.} \;\; Q_k \le P_k \tag{12a}$$

$$t + \sum_{k=1}^{K} b_k t_0 \le T \tag{12b}$$

where $\mathbf{a} = [D_1 lnQ_1, \ldots, D_K lnQ_K]^T$, $\mathbf{b} = [b_1, \ldots, b_K]^T$, and $\mathbf{A} = \text{diag}[(lnQ_1)^2 \cdot D_1/2, \ldots, (lnQ_K)^2 \cdot D_K/2]$. From problem (12), we observe that the nonconvex problem is transformed into a convex problem. Then, we obtain the optimal solution of the original problem by comparing the objective function value of the integer solution near the optimal solution of the relaxation problem. The optimization method for solving the problem (12) is summarized in Algorithm 3.

For comparison, the enumeration method is used to solve this integer programming problem. The specific iterative process is summarized in Algorithm 4. Besides, for the convex optimization process in Algorithms 3 and 4, we utilize the interior-point method.

Algorithm 3 Quadratic Approximation Method

Initialze, $b_k = 1$, $k = 1, \ldots$,K, $\mathbf{b} = [b_1, \ldots, b_K]^T$, $\mathbf{b} = argmin(y_2)$, $\mathbf{bl} = \lfloor \mathbf{b} \rfloor$, $\mathbf{bh} = \lceil \mathbf{b} \rceil$, $\mathbf{bA} = [\mathbf{bl}, \mathbf{bh}]$.
for $j_1, \ldots, j_K \in \{1, 2\}$ **do**
while $t + \sum_{k=1}^{K} b_k * t_0 < T$ **and** $Q_k \leqslant P_k$ **do**
  $b_1 = \mathbf{bA}(1, j_1)$,
  $\vdots$
  $b_K = \mathbf{bA}(K, j_K)$.
  if $y_{before} \leqslant y_{update}$
    $y = y_{update}$
    Update $\mathbf{b}$
  endif
endwhile
endfor
output $\mathbf{b}_{opt}$=$\mathbf{b}$.

Algorithm 4 Enumeration Method

Initialize $b_k = 1$, $k = 1, \ldots$,K, $b_{max} = max\{b_1, \ldots, b_K\}$, $\mathbf{b} = [b_1, \ldots, b_K]^T$.
repeat
  Update the maximum value of perception times
    $bmax = \lfloor (T - t)/t0 - K + 1 \rfloor$.
  for $b_1, \ldots, b_K \in \{1, \ldots, b_{max}\}$ **do**
  while $t + \sum_{k=1}^{K} b_k * t_0 < T$ **and** $Q_k \leqslant P_k$ **do**
    if $y_{before} \leqslant y_{update}$
      $y = y_{update}$
      Update $\mathbf{b}$
  endwhile
  endfor
until Objective value converges.

C. Optimization Analysis of 3D-RIS.

The coordinate descent method is utilized for problem (6). The detailed steps of this method are presented in the following.

First, we adopt a utility function

$$y_{m_i} = y_{\boldsymbol{x}_i} - y_{\boldsymbol{x}} \tag{13}$$

where $\boldsymbol{x}_i$ represents the switching sequence after the update, and $\boldsymbol{x}$ represents the switching sequence before the update. The updating rule of the switch sequence is given by

$$\boldsymbol{x}_i = [x_1, \ldots, x_i \oplus 1, \ldots, x_N]^T. \tag{14}$$

In the iteration process, we will change the switch state of the i^*th element, where i^* is derived as

$$i^* = \arg\max_i \left\{\mathbf{y}_m\right\} \tag{15}$$

where $\mathbf{y}_m = [y_{m_1}, \ldots, y_{m_N}]^T$. The algorithm for solving problem (6) is summarized in Algorithm 5. Finally, the algorithm to solve problem (5) is summarized in Algorithm 6. The interior-point method is used in the iterative process.

D. Complexity Analysis

According to Algorithm 1, to solve problem (8), the complexity lies in computing the next iteration point $\boldsymbol{v}_j$, which

Algorithm 5 Coordinate Descent Method

Initialize $\boldsymbol{x} = [1, \ldots, 1]^T$, $\mathbf{y}_m = [y_{m_1}, \ldots, y_{m_N}]^T$
repeat
  for $i = 1 : N$
    $\boldsymbol{x}_i = [x_1, \ldots, x_i \oplus 1, \ldots, x_N]^T$,
    Calculation $y_{m_i} = y_{\boldsymbol{x}_i} - y_{\boldsymbol{x}}$
  endfor
    Update $i^* = \underset{i}{\operatorname{argmax}} \{\mathbf{y}_m\}$
  if $y_{x_{i^*}} > 0$
    Update $\boldsymbol{x} = [x_1, \ldots, x_{i^*} \oplus 1, \ldots, x_N]^T$
until Objective value converges.

Algorithm 6 Iterative Optimization for Problem (5)

Initialize $(\boldsymbol{\theta}_{(0)}, \boldsymbol{b}_{(0)}, \boldsymbol{x}_{(0)})$, Set iteration number n = 1.
repeat
  Given $\boldsymbol{\theta}_{(n-1)}$, the optimized $\boldsymbol{\theta}$ is obtained by Algorithm 1 and denoted by $\boldsymbol{\theta}_{(n)}$.
  Given $\boldsymbol{\theta}_{(n)}$ and $\boldsymbol{x}_{(n-1)}$, the optimization problem (6) is solved by using Algorithm 5 and the solution is denoted by $\boldsymbol{x}_{(n)}$.
  Given $\boldsymbol{\theta}_{(n)}$, $\boldsymbol{x}_{(n)}$ and $\boldsymbol{b}_{(n-1)}$, we solve the optimization problem (5) according Algorithm 3.
  Set $n = n + 1$.
until The objective value converges.

TABLE II
PARAMETER SETTINGS

Number	Application	Numerical	Unit
1	BS transmit power	50	dBm
2	Background noise power	-104	dBm
3	Bandwidth	1	MHz
4	Circuit power of the DC	39	dBm
5	Circuit power of BS	80	dBm
6	Power of a RIS element	10	dBm

involves the complexity of $\mathcal{O}(N)$. Algorithm 2 is dominated by the complexity of the alternating process, where the number of iterations increases sharply and is represented by S, so the complexity is $\mathcal{O}(NS)$. In Algorithm 3, the complexity of the quadratic approximation method for solving problem (12) is $\mathcal{O}(2^N)$. N represents the number of variables, and each variable can be converted between two values. According to Algorithm 4, all states of the variable need to be traversed one by one. N variables require close to N^N iterations. So, the enumeration method in Algorithm 4 involves the complexity of $\mathcal{O}(N^N)$. The number of iterations decreases gradually in solving problem (6). N variables require $N!$ iterations. So, the complex for the coordinate descent method in Algorithm 5 is $\mathcal{O}(N!)$.

V. Simulation Results and Discussion

This section provides the simulation results to verify the theoretical findings. The parameter settings [34] are summarized in Table II.

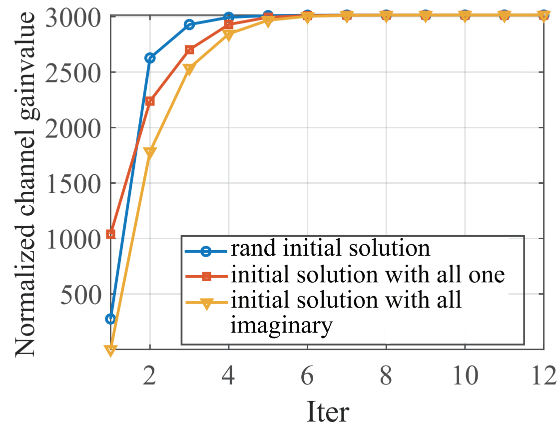

Fig. 3. Convergence behavior of Algorithm 1 with different initial solutions.

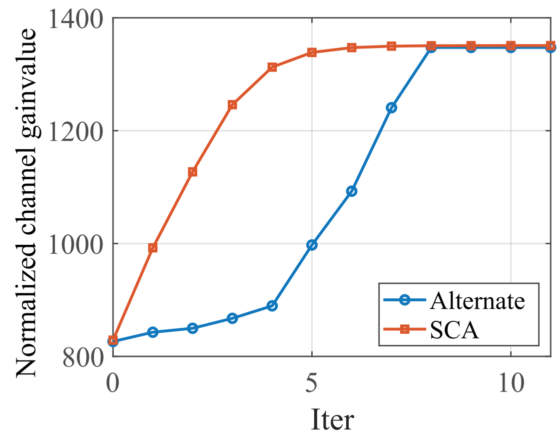

Fig. 4. Comparisons of convergence results of Algorithms 1 and 2.

A. Phase-Shift Matrix Optimization

This experiment uses the iterative method based on SCA to solve the RIS problem (8). $\boldsymbol{\theta}$ in the experiment are set to random values, all one and all zero. The variation curves between the normalized channel gain value and the number of iterations are shown in Fig. 3, where the normalized channel gain represents the ratio of channel gain to the noise power, denoted by $|g + U^H v|^2/\sigma^2$.

As observed in Fig. 3, Algorithm 1 converges within ten iterations. In addition, we compare the SCA method with the alternative optimization method. The convergence curves of the alternating optimization and the SCA methods are shown in Fig. 4. In Fig. 4, Alternate means the objective value by utilizing the alternating optimization method. The horizontal coordinate corresponding to the alternating optimization in Fig. 4 is the number of updates of the objective function values rather than the number of iterations. We can see that after a finite number of iterations, two methods have converged, and the optimal function value is stable. However, alternative optimizations require more iterations to converge.

B. Perceptual Time Optimization

We show the results of Algorithms 3 and 4 in Figs. 5 and 6, respectively. In Figs. 5 and 6, before optimize means the

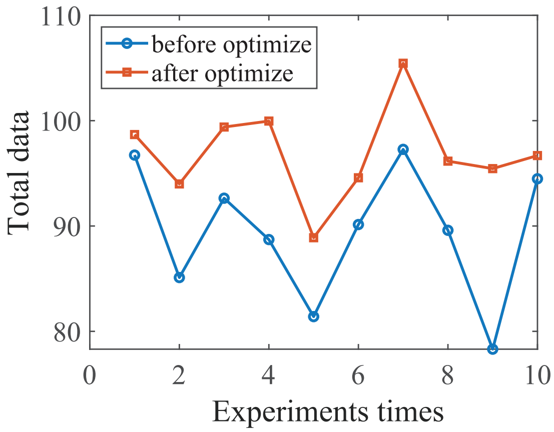

Fig. 5. Optimization results of Algorithm 3 versus multiple simulation times.

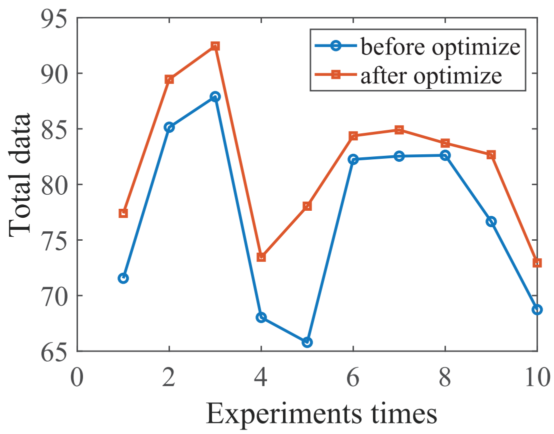

Fig. 6. Optimization results of Algorithm 4 versus multiple simulation times.

objective value with random solution, while after optimize means the objective value with the optimal solution. In both figures, we show the objective values with various random settings. According to these two figures, we can find that the optimization of Algorithms 3 and 4 is correct.

In Fig. 5, we compare the optimization results of ten tests. K is fixed as 5, and the objective function is the perceived total data. The total data after optimization is significantly larger than that before optimization. According to Algorithm 3, the optimal solution is feasible.

Fig. 6 compares function values before and after optimization using the enumeration method similar to Fig. 5. The objective function value increases obviously after optimization. Therefore, the feasibility of the enumeration method is verified.

Fig. 7 shows how the perceived data changes as the data update time T varies for the quadratic approximation and enumeration methods. Here, for precise comparison, we set K as 8. There is almost no difference between the convergence results of the two methods because the quadratic approximation method approximates the original function. With the increase in T, there might be some errors.

Fig. 8 shows the perceived data versus the area perception times, where we let $T = 20 \times K$ based on experience. From this figure, we notice that the two methods almost converge

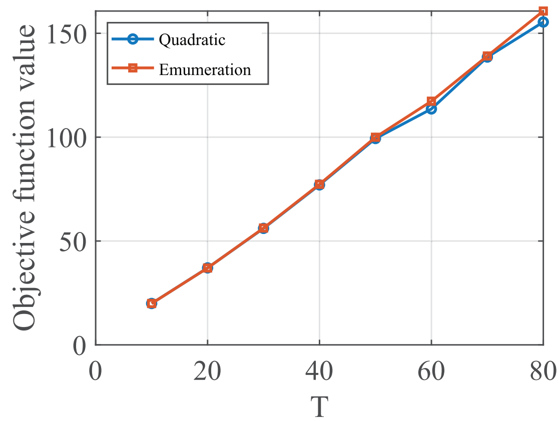

Fig. 7. Convergence comparison of two methods with different T.

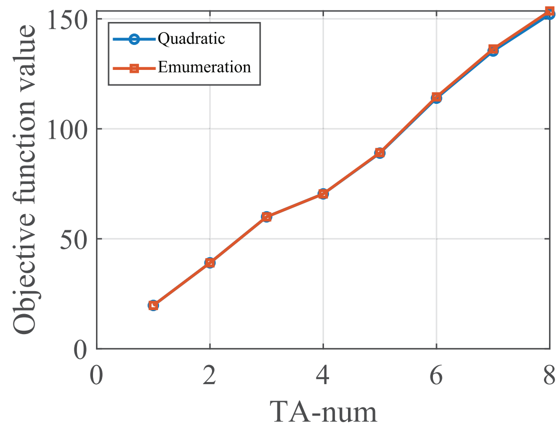

Fig. 8. Convergence comparison of two methods when the number of regions to be perceived is different.

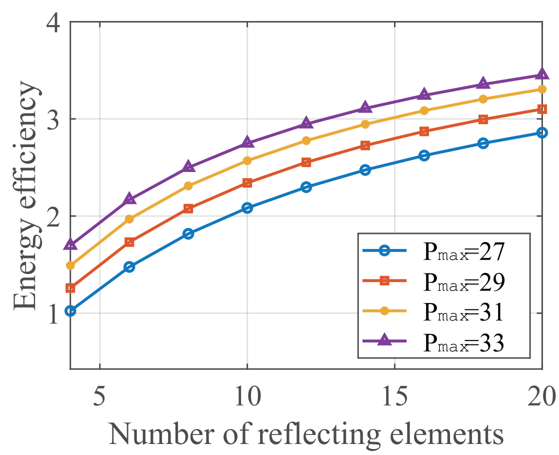

Fig. 9. Relationship between energy efficiency and RIS element number under different power.

to the same result, similar to Fig. 7. Thus, we verify that the quadratic approximation method can solve problem (12) with low complexity.

Fig. 9 shows the curves of the energy efficiency (defined as the ratio of spectral efficiency over power consumption) and the number of RIS elements under various values of powers. It can be seen from Fig. 9 that the energy efficiency increases

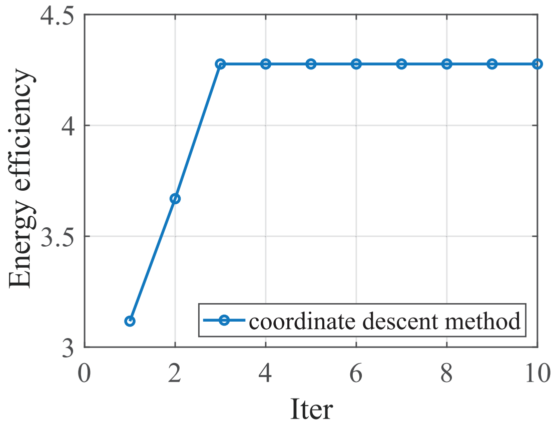

Fig. 10. Influence of RIS element switch on energy efficiency.

significantly with the increase in power and the number of RIS elements. Simultaneously, with the increase in RIS elements, the energy consumption for RIS is also higher.

Furthermore, we improve energy efficiency by turning off some elements. We set the RIS element to 100 and use the coordinate descent method to optimize the RIS element switches. The simulation results are shown in Fig. 10. We can see that the algorithm has reached convergence, and the energy efficiency has improved. This result shows that the energy consumed by RIS to regulate the phase cannot be ignored when there are many RIS elements. We can improve energy efficiency by finding the optimal RIS element switching sequence.

VI. Conclusion

In this article, we investigated the problem of resource allocation in the RIS-assisted coal mine JCAS system. RIS phase-shift matrix, areas sensing times, and RIS element switch matrix were jointly optimized to sense as much secure data as possible while meeting the maximum data update time, maximum power, minimum area sensing demands, and unit-modulus constraints. In order to solve this problem, we used the SCA-based iterative algorithm to optimize the RIS phase-shift matrix and the Taylor quadratic approximation method to optimize the times of area perception. Simulation results showed that time-division sensing and communication are feasible for security checks, and using RIS to assist wireless communication in the coal mine is feasible.

References

[1] Y. Cui, F. Liu, X. Jing, and J. Mu, "Integrating sensing and communications for ubiquitous IoT: Applications, trends and challenges," 2021, *arXiv:2104.11457*.

[2] S. Zhang, H. Zhang, L. Song, Z. Han, and H. V. Poor, "Sensing and communication tradeoff design for AoI minimization in a cellular Internet of UAVs," in *Proc. IEEE Int. Conf. Commun. (ICC)*, 2020, pp. 1–6.

[3] C. Wang et al., "mmPhone: Acoustic eavesdropping on loudspeakers via mmWave-characterized piezoelectric effect," in *Proc. IEEE INFOCOM Conf. Comput. Commun. (IEEE INFOCOM)*, 2022, pp. 820–829.

[4] M. Vogt, J. Opretzka, and H. Ermert, "Synthetic aperture focusing technique for high-resolution imaging of surface structures with high-frequency ultrasound," in *Proc. IEEE Int. Ultrasonics Symp. (IEEE IUS)*, 2009, pp. 1514–1517.

[5] F. Liu, C. Masouros, A. P. Petropulu, H. Griffiths, and L. Hanzo, "Joint radar and communication design: Applications, state-of-the-art, and the road ahead," *IEEE Trans. Commun.*, vol. 68, no. 6, pp. 3834–3862, Jun. 2020.

[6] X. You et al., "Towards 6G wireless communication networks: Vision, enabling technologies, and new paradigm shifts," *Sci. China Inf. Sci.*, vol. 64, no. 1, pp. 1–74, 2021.

[7] S. Piao, Z. Ba, L. Su, D. Koutsonikolas, S. Li, and K. Ren, "Automating CSI measurement with UAVs: From problem formulation to energy-optimal solution," in *Proc. IEEE Conf. Comput. Commun. (IEEE INFOCOM)*, 2019, pp. 2404–2412.

[8] Q. Wu, Y. Zhao, Q. Fan, P. Fan, J. Wang, and C. Zhang, "Mobility-aware cooperative caching in vehicular edge computing based on asynchronous federated and deep reinforcement learning," *IEEE J. Sel. Topics Signal Process.*, early access, Nov. 10, 2022, doi: 10.1109/JSTSP.2022.3221271.

[9] Y. Ye, L. Shi, X. Chu, G. Lu, and S. Sun, "Mutualistic cooperative ambient backscatter communications under hardware impairments," *IEEE Trans. Commun.*, vol. 70, no. 11, pp. 7656–7668, Nov. 2022.

[10] Q. Wu, S. Shi, Z. Wan, Q. Fan, P. Fan, and C. Zhang, "Towards V2I age-aware fairness access: A DQN based intelligent vehicular node training and test method," 2022, *arXiv:2208.01283*.

[11] Y. Ye, L. Shi, X. Chu, R. Q. Hu, and G. Lu, "Resource allocation in backscatter-assisted wireless powered MEC networks with limited MEC computation capacity," *IEEE Trans. Wireless Commun.*, vol. 21, no. 12, pp. 10678–10694, Dec. 2022.

[12] X. Tong et al., "Environment sensing considering the occlusion effect: A multi-view approach," *IEEE Trans. Signal Process.*, vol. 70, pp. 3598–3615, 2022.

[13] K. Yang, Y. Shi, Y. Zhou, Z. Yang, L. Fu, and W. Chen, "Federated machine learning for intelligent IoT via reconfigurable intelligent surface," *IEEE Netw.*, vol. 34, no. 5, pp. 16–22, Sep. 2020.

[14] M. Fu, Y. Zhou, Y. Shi, and K. B. Letaief, "Reconfigurable intelligent surface empowered downlink non-orthogonal multiple access," *IEEE Trans. Commun.*, vol. 69, no. 6, pp. 3802–3817, Jun. 2021.

[15] Y. Xiu et al., "Reconfigurable intelligent surfaces aided mmWave NOMA: Joint power allocation, phase shifts, and hybrid beamforming optimization," *IEEE Trans. Wireless Commun.*, vol. 20, no. 12, pp. 8393–8409, Dec. 2021.

[16] W. Ni, Y. Liu, Y. C. Eldar, Z. Yang, and H. Tian, "STAR-RIS integrated nonorthogonal multiple access and over-the-air federated learning: Framework, analysis, and optimization," *IEEE Internet Things J.*, vol. 9, no. 18, pp. 17136–17156, Sep. 2022.

[17] Z. Yang et al., "Energy-efficient wireless communications with distributed reconfigurable intelligent surfaces," *IEEE Trans. Wireless Commun.*, vol. 21, no. 1, pp. 665–679, Jan. 2022.

[18] X. U. Yongjun, Z. Yang, C. Huang, Y. Chau, and G. Gui, "Resource allocation for two-tier RIS-assisted heterogeneous NOMA networks," *ZTE Commun.*, vol. 20, no. 1, p. 12, 2022.

[19] C. Huang, A. Zappone, G. C. Alexandropoulos, M. Debbah, and C. Yuen, "Reconfigurable intelligent surfaces for energy efficiency in wireless communication," *IEEE Trans. Wireless Commun.*, vol. 18, no. 8, pp. 4157–4170, Aug. 2019.

[20] C. Huang et al., "Hybrid beamforming for RIS-empowered multi-hop terahertz communications: A DRL-based method," in *Proc. IEEE Globecom Workshops (GC Wkshps)*, 2020, pp. 1–6.

[21] I. F. Akyildiz, C. Han, and S. Nie, "Combating the distance problem in the millimeter wave and terahertz frequency bands," *IEEE Commun. Mag.*, vol. 56, no. 6, pp. 102–108, Jun. 2018.

[22] M. Li and Y. Liu, "Underground coal mine monitoring with wireless sensor networks," *ACM Trans. Sensor Netw.*, vol. 5, no. 2, pp. 1–29, 2009.

[23] L. Muduli, P. K. Jana, and D. P. Mishra, "A novel wireless sensor network deployment scheme for environmental monitoring in longwall coal mines," *Process Safety Environ. Protect.*, vol. 109, pp. 564–576, Jul. 2017.

[24] X. Xusheng, M. Kun, M. Hongwei, S. Wanfeng, and F. Hongwei, "Analysis of wireless electromagnetic wave propagation mechanism for coal mine rescue robot," in *Proc. IEEE Int. Conf. Real Time Comput. Robot. (RCAR)*, 2018, pp. 64–67.

[25] I. B. Mabrouk, J. Hautcoeur, L. Talbi, M. Nedil, and K. Hettak, "Feasibility of a millimeter-wave MIMO system for short-range wireless communications in an underground gold mine," *IEEE Trans. Antennas Propag.*, vol. 61, no. 8, pp. 4296–4305, Aug. 2013.

[26] G. Brooker, J. Martinez, and R. Hennessey, "Millimetre wave radar imaging of mining vehicles," in *Proc. 7th Eur. Radar Conf. (EuRAD)*, 2010, pp. 284–287.

[27] G. Brooker, E. Widzyk-Capehart, S. Scheding, R. Hennessy, and C. Lobsey, "Millimetre wave radar visualisation in mines," in *Proc. Eur. Radar Conf. (EuRAD)*, 2007, pp. 417–420.

[28] M. Leingartner, J. Maurer, G. Steinbauer, and A. Ferrein, "Evaluation of sensors and mapping approaches for disasters in tunnels," in *Proc. IEEE Int. Symp. Safety Security Rescue Robot. (SSRR)*, 2013, pp. 1–7.

[29] R. M. Mealey, "A method for calculating error probabilities in a radar communication system," *IEEE Trans. Space Electron. Telemetry*, vol. SET-9, no. 2, pp. 37–42, Jun. 1963.

[30] A. Hassanien, M. G. Amin, Y. D. Zhang, and F. Ahmad, "Dual-function radar-communications: Information embedding using Sidelobe control and waveform diversity," *IEEE Trans. Signal Process.*, vol. 64, no. 8, pp. 2168–2181, Apr. 2016.

[31] C. Jiao, Z. Zhang, C. Zhong, X. Chen, and Z. Feng, "Millimeter wave communication with active ambient perception," *IEEE Trans. Wireless Commun.*, vol. 18, no. 5, pp. 2751–2764, May 2019.

[32] J. Yao, Z. Zhang, X. Shao, C. Huang, C. Zhong, and X. Chen, "Concentrative intelligent reflecting surface aided computational imaging via fast block sparse Bayesian learning," in *Proc. IEEE 93rd Veh. Technol. Conf. (VTC-Spring)*, 2021, pp. 1–6.

[33] Y. Tao and Z. Zhang, "Distributed computational imaging with reconfigurable intelligent surface," in *Proc. Int. Conf. Wireless Commun. Signal Process. (WCSP)*, 2020, pp. 448–454.

[34] M. Chen, Z. Yang, W. Saad, C. Yin, H. V. Poor, and S. Cui, "A joint learning and communications framework for federated learning over wireless networks," *IEEE Trans. Wireless Commun.*, vol. 20, no. 1, pp. 269–283, Jan. 2021.

Tianhao Guo (Member, IEEE) received the Ph.D. degree from the School of Electronic Engineering and Computer Science, Queen Mary University of London, London, U.K., in 2020.

He is currently a Lecturer with Shanxi University, Taiyuan, China. He is also the Postdoctoral Research Associate with the National Key Laboratory of Integrated Services Networks, Xidian University, Xi'an, China. His research interests include semantic and pragmatic communication, reconfigurable intelligent-surface-aided joint communication and sensing in coal mines, and deep learning technologies for wireless communications.

Dr. Gou is also serving as a Review Editor for the *Frontiers in Space Technologies* and *Frontiers in Computer Science*. He has served as a Workshop Co-Chair of ICSINC Big Data Workshop 2021. He has reviewed papers from IEEE WIRELESS COMMUNICATIONS and *Wireless Communications and Mobile Computing*.

Xianzhong Li received the B.S. degree in science and technology of electronic information from Shanxi University, Taiyuan, China, in 2020, where he is currently pursuing the M.S. degree in information and communication engineering.

Muyu Mei received the B.S. degree in applied mathematics from Xidian University, Xi'an, China, in 2017, where he is currently pursuing the Ph.D. degree in information and communication systems.

His research interests include performance analysis and stochastic optimization for large-scale wireless networks and multihop ad hoc networks.

Zhaohui Yang (Member, IEEE) received the B.S. degree in information science and engineering from Chien-Shiung Wu Honors College, Southeast University, Nanjing, China, in June 2014, and the Ph.D. degree in communication and information system with National Mobile Communications Research Laboratory, Southeast University in May 2018.

He was a Postdoctoral Research Associate with the Center for Telecommunications Research, Department of Informatics, King's College London, London, U.K., from 2018 to 2020. He was a Research Fellow with the Department of Electronic and Electrical Engineering, University College London, London, from 2020 to 2022. He is currently a ZJU Young Professor with the College of Information Science and Electronic Engineering, Zhejiang Key Laboratory of Information Processing Communication and Networking, Zhejiang University, Hangzhou, China, and also a Research Scientist with Zhejiang Laboratory, Hangzhou. His research interests include joint communication, sensing, and computation, federated learning, reconfigurable intelligent surface, UAV, and NOMA.

Prof. Yang is an Associate Editor for the IEEE COMMUNICATIONS LETTERS, IET COMMUNICATIONS, and *EURASIP Journal on Wireless Communications and Networking*. He has Guest Edited a feature topic of *IEEE Communications Magazine* on Communication Technologies for Efficient Edge Learning and a special issue of IEEE JOURNAL ON SELECTED AREAS IN COMMUNICATIONS for Beyond Transmitting Bits: Context, Semantics and Task-Oriented Communications. He was a Co-Chair for international workshops with more than ten times, including ICC, GLOBECOM, WCNC, PIMRC, and INFOCOM. He was a TPC member of IEEE ICC from 2015 to 2022 and GLOBECOM from 2017 to 2022. He was an Exemplary Reviewer for IEEE TRANSACTIONS ON COMMUNICATIONS in 2019 and 2020.

Jia Shi (Member, IEEE) received the M.Sc. and Ph.D. degrees from the University of Southampton, Southampton, U.K., in 2010 and 2015, respectively.

He was a Research Associate with Lancaster University, Lancaster, U.K., from 2015 to 2017. He became a Research Fellow with 5GIC, University of Surrey, Guildford, U.K., from 2017 to 2018. He has been with Xidian University, Xi'an, China, since 2018, where he is currently an Associate Professor with the National Key Laboratory of Integrated Services Networks. His current research interests include resource allocation in wireless systems, covert communications, physical-layer security, mmWave communications, and satellite communications.

Prof. Shi is also serving as an Associate Editor for the *Electronic Letters*, and an Editor for the *International Journal of Communications System*. He is serving as a Guest Editor for the *China Communications*.

Kai-Kit Wong (Fellow, IEEE) received the B.Eng., M.Phil., and Ph.D. degrees in electrical and electronic engineering from Hong Kong University of Science and Technology, Hong Kong, in 1996, 1998, and 2001, respectively.

After graduation, he took up the Academic and Research positions with the University of Hong Kong, Hong Kong; Lucent Technologies, Murray Hill, NJ, USA; Bell-Labs, Holmdel, NJ, USA; the Smart Antennas Research Group, Stanford University, Stanford, CA, USA; and the University of Hull, Hull, U.K. He is a Chair of Wireless Communications with the Department of Electronic and Electrical Engineering, University College London, London, U.K. His current research centers around 5G and beyond mobile communications.

Prof. Wong is a co-recipient of the 2013 IEEE SIGNAL PROCESSING LETTERS Best Paper Award and the 2000 IEEE VTS Japan Chapter Award at the IEEE Vehicular Technology Conference in Japan in 2000, and a few other international best paper awards. He has been the Editor-in-Chief for the IEEE WIRELESS COMMUNICATIONS LETTERS since 2020. He is a Fellow of IET and is also on the editorial board of several international journals.

Zhaoyang Zhang (Senior Member, IEEE) received the Ph.D. degree from Zhejiang University, Hangzhou, China, in 1998.

He is currently a Qiushi Distinguished Professor with Zhejiang University. His research interests include fundamental aspects of wireless communications and networking, such as information theory and coding theory, network signal processing and distributed learning, AI-empowered communications and networking, and synergetic sensing, computing, and communication.

Prof. Zhang was awarded the National Natural Science Fund for Distinguished Young Scholars by NSFC in 2017. He has coauthored more than 300 peer-reviewed international journals and conference papers, including eight conference best papers awarded by IEEE ICC 2019 and IEEE GlobeCom 2020. He was also a Keynote Speaker for APCC 2018 and VTC-Fall 2017 Workshop NOMA. He is serving or has served as an Editor for the IEEE TRANSACTIONS ON WIRELESS COMMUNICATIONS, IEEE TRANSACTIONS ON COMMUNICATIONS, and *IET Communications*, and the General Chair, the TPC Co-Chair, or the Symposium Co-Chair for PIMRC 2021 Workshop on Native AI Empowered Wireless Networks, VTC-Spring 2017 Workshop on HMWC, WCSP 2013/2018, and Globecom 2014 Wireless Communications Symposium.